

# Active Flow Control on the Stingray Uninhabited Air Vehicle: Transient Behavior

Michael Amitay\*

Rensselaer Polytechnic Institute, Troy, New York 12180

Anthony E. Washburn<sup>†</sup> and Scott G. Anders<sup>‡</sup>

NASA Langley Research Center, Hampton, Virginia 23681

and

David E. Parekh<sup>§</sup>

Georgia Tech Research Institute, Atlanta, Georgia 30080

The application of leading-edge separation control on an uninhabited air vehicle (UAV) with 50-deg leading-edge sweep is investigated experimentally in a full-scale close-return wind tunnel using arrays of synthetic jet actuators. Active flow control is used to enhance vehicle control at moderate and high angles of attack for takeoff and landing activities or gust load alleviation. The surface-mounted synthetic jet actuators are operated in various waveforms where the carrier frequency is at least an order of magnitude higher than the characteristic shedding frequency of the UAV. Actuation yields a suction peak near the leading edge, however, while excitation with a sinusoidal waveform results in a sharp suction peak near the leading edge; pulse modulation yields a larger and wider suction peak. The flow transients associated with controlled reattachment and separation of the flow over the UAV are investigated using amplitude modulation of the actuation waveform by measuring the dynamic surface pressure at different locations on the upper surface of the UAV's wing. Phase-locked measurements show that the transients, associated with the onset of reattachment and separation, at high angles of attack are accompanied by the shedding of large-scale vortical structures and oscillations of the surface pressure. However, no oscillations are observed when the baseline flow is attached.

## Nomenclature

$\bar{A}_w$	= wing mean area, $\frac{1}{2}b \cdot \bar{c}$ , m <sup>2</sup>
$b$	= wing span, m
$b_j$	= synthetic jet slot width, m
$C_l$	= rolling moment
$C_m$	= pitching moment
$C_p$	= pressure coefficient
$C_\mu$	= unsteady jet-momentum coefficient, $n \cdot \bar{I}_j / \frac{1}{2}\rho \cdot U_\infty^2 \cdot \bar{A}_w$
$c$	= airfoil chord, m
$c_r$	= root chord, m
$\bar{c}$	= mean aerodynamic chord, m
$f_c$	= carrier frequency, Hz
$f_{\text{mod}}$	= frequency of modulation, Hz
$f_{\text{tof}}$	= time of flight defined as $f_{\text{tof}} = U_\infty / \bar{c}$
$h_j$	= synthetic jet slot width, m
$\bar{I}_j$	= time-averaged momentum associated with the synthetic jet discharge, $\frac{1}{\tau} \rho_j \cdot b_j \cdot l_j \cdot \int_0^\tau \langle u_j^2(t) \rangle dt$
$l_j$	= synthetic jet slot length, m
$n$	= number of synthetic jets
$Re_{\bar{c}}$	= Reynolds number based on mean chord

Presented as Paper 2003-4001 at the AIAA 33rd Fluid Dynamics Conference, Orlando, FL, 23–26 June 2003; received 8 October 2003; revision received 19 April 2004; accepted for publication 13 May 2004. Copyright © 2004 by the American Institute of Aeronautics and Astronautics, Inc. All rights reserved. Copies of this paper may be made for personal or internal use, on condition that the copier pay the \$10.00 per-copy fee to the Copyright Clearance Center, Inc., 222 Rosewood Drive, Danvers, MA 01923; include the code 0001-1452/04 \$10.00 in correspondence with the CCC.

\*Assistant Professor, Department of Mechanical, Aerospace and Nuclear Engineering, 110 8th Street; amitam@rpi.edu. Senior Member AIAA.

†Research Engineer, Flow Physics and Control Branch. Senior Member AIAA.

‡Research Engineer, Flow Physics and Control Branch.

§Deputy Director. Senior Member AIAA.

$Sr_{\bar{c}}$	= Strouhal number based on mean chord
$T_{305}$	= period of the carrier (305 Hz) frequency, s
$t$	= time, s
$u_j(t)$	= jet exit velocity, m/s
$U_\infty$	= freestream velocity, m/s
$x$	= distance from leading edge, m
$\alpha$	= angle of attack, deg
$\Delta C_p$	= increment in $C_p$ caused by actuation with respect to the baseline case
$\delta_f$	= flap-deflection angle, deg
$\Lambda_{\text{LE}}$	= leading-edge sweep angle, deg
$\rho$	= freestream density
$\rho_j$	= synthetic jet density
$\tau$	= time of the synthetic jet discharge, $T_{305}/2$

## I. Introduction

ACTIVE flow control holds tremendous promise for expanding the performance of current vehicles and enabling revolutionary concepts for advanced vehicle designs. Realization of that promise requires focused research and design (R&D) efforts to move the technology from the laboratory to flight. Acceptance of this technology for commercial aircraft and for uninhabited air vehicles (UAVs) operating in civilian airspace will be possible once major advances in the technology readiness of active flow control are achieved.

The present work deals with advancing this technology by moving from previous subscale laboratory research toward a full-scale flight demonstration on an existing UAV platform nicknamed "Stingray" and based on the Air Force 1301 UAV design. This UAV technology demonstrator, designed, built, and flown by Boeing Phantom Works, has a 2.8-m wing span, a design mass of 36 kg, and a maximum design speed of 129 m/s (250 kn). The aircraft has a six-component-gyro instrumentation package, onboard data recorder, and wireless downlink to enable in-flight measurements of the aircraft's performance and can accommodate a full flight control computer system. Split flaps are used to control the vehicle conventionally. The wing panels are removable for the installation of electronic flight controls and active flow control devices. The bolt-on skins allow for installation of sensors and actuators.

Control of separation has been typically achieved by exploiting the combined narrowband receptivity the separating shear layer and the upstream boundary layer to external actuation (e.g., Ref. 1). Oster and Wygnanski<sup>2</sup> and Roberts<sup>3</sup> showed that the actuation can affect the global flowfield by modifying the evolution and interactions of the large-scale vortical structures. These modifications can lead to a Coanda-like deflection of the separating shear layer toward the surface (e.g., Ref. 4) such that the layer vortices are advected downstream in close proximity to the surface.

This approach has been implemented, with varying degrees of success, to restore aerodynamic performance of stalled airfoils and flaps (e.g., Refs. 5–7). In particular, Seifert et al.<sup>7</sup> and Wygnanski<sup>8</sup> argued that the actuation is most effective when its period scales with the advection time over the length of the flow domain downstream of separation as measured by the reduced frequency  $F^+$ . Therefore, when the separation domain scales with the characteristic length of an aerodynamic body the (dimensionless) actuation frequency can couple to, and even drive, the shedding frequency in the near wake. The possibility of coupling (or feedback) between (nominally) time-periodic shedding of coherent vortices and the separated shear layer in the absence of actuation is intriguing because such feedback between the near-wake instabilities and the separating shear layer is even more pronounced in the presence of actuation thereby amplifying the unsteady component of the global aerodynamic forces. A discussion on these effects was presented by Amitay and Glezer.<sup>9,10</sup>

Amitay et al.<sup>11</sup> presented a different approach to the control of flow separation on lifting surfaces by using synthetic jet actuators operating at high frequencies (at least an order of magnitude higher than the characteristic frequency of the flow). This type of actuation emphasize fluidic modification of the “apparent” aerodynamic shape of the surface upstream of separation, which alters the streamwise pressure gradient resulting in a complete or partial suppression of separation. Because the synthetic jet is synthesized from the surrounding fluid (for more details, see Smith and Glezer,<sup>12</sup> the review paper by Glezer and Amitay,<sup>13</sup> and Cater and Soria<sup>14</sup>), when it is placed near a surface its interaction with the embedded flow can result in the formation of a controlled interaction domain between the a synthetic jet and the crossflow above the surface. The modification of the apparent shape of aerodynamic surfaces has been exploited for controlling the evolution of both wall-bounded and free shear flows (e.g., stalled airfoils<sup>9</sup> and jet vectoring,<sup>15</sup> respectively) and small-scale UAVs.<sup>16,17</sup>

The flow transients associated with controlled reattachment and separation of the flow over a stalled two-dimensional airfoil were investigated by Amitay and Glezer<sup>10</sup> and Smith et al.<sup>18</sup> in wind-tunnel experiments. The transients associated with flow reattachment and separation were investigated using amplitude modulation of the actuation waveform. Using phase-locked measurements of the velocity field in the near wake of the airfoil and corresponding flow visualizations, they showed that the transients that are associated with the onset of reattachment and separation are accompanied by the shedding of large-scale vortical structures and oscillations of the circulation. Similar results on an inclined flat plate were obtained by Darabi and Wygnanski.<sup>19,20</sup>

In the present paper we implemented a new method that was first introduced by Amitay and Glezer<sup>10</sup> and Smith et al.<sup>18</sup>: the pulsed modulated actuation of the actuation waveform (similar experiments were conducted on a circular cylinder by Naim et al.<sup>21</sup> and on a supercritical airfoil by Pack et al.<sup>22</sup>). They showed that by exploiting the flow transients that are associated with the onset and removal of the actuation the performance of the actuators at reduced levels of momentum coefficient, can be substantially enhanced by pulse modulation of their resonance waveform (nominally at  $Sr_{\bar{c}} = 10$ ). Using this actuation method, the lift was further augmented compared to that obtained by conventional time-harmonic actuation.

The flow control technology presented in the present paper involves control of aerodynamic performance (i.e., forces and moments) of the vehicle via embedded synthetic jet actuators in the leading edges. These embedded resonant actuators are intended to control separated flows through the introduction of a time-dependent momentum flux that interacts with the separated shear layer. The im-

plementation of leading-edge separation control was chosen for this vehicle to enhance vehicle control at relatively high angles of attack and at low speeds. The vehicle has 50 deg of leading-edge sweep and airfoil profiles with fairly blunt leading edges. This results in a flowfield regime somewhere in between mildly swept quasi-two-dimensional flows and highly swept delta-wing flows. Leading-edge zero-net mass active control has been previously demonstrated in both two-dimensional and delta-wing flowfields. Significantly, Margalit et al.<sup>23</sup> surmise that the control they achieved on a 60-deg sharp-edge delta wing was caused by a quasi-two-dimensional mechanism. The approach taken herein also attempts to effect control through a quasi-two-dimensional input along the leading edge.

## II. Experimental Setup

The ultimate objective of the present work is the flight demonstration of vehicle dynamic control through active flow control (with closed-loop feedback) on a low-speed UAV. In the first stage of this project, the baseline and active flow control enhanced aerodynamic performance of the full-scale Stingray UAV (Fig. 1) were measured in wind-tunnel testing. These tests were conducted in the NASA Langley Research Center Transonic Dynamics Tunnel. The tunnel is a subatmospheric transonic facility with a 4.88-m test section. The Stingray model (having a wing span of 2.8 m and a root chord of 2 m; see Fig. 2) was tested between 14 to 24 deg angle-of-attack range. The mean chord Reynolds numbers  $Re_{\bar{c}}$  (based on the mean chord and the freestream velocity) varied between  $8.25 \times 10^5$  and  $2.07 \times 10^6$  with velocities of 15 and 40 m/s, respectively.

As mentioned earlier, the leading edge of each wing is instrumented with an array of synthetic (zero-mass flux) jet actuators, where the leading edge slot is divided into eight individually addressable sections (Fig. 3). Each section is 142 mm long and 0.76 mm wide and was powered by two 63.5-mm piezoelectric disks. (These disks are driven by an ac voltage to produce the periodic motion, which is essential to the formation of the synthetic jet.) As shown in Fig. 2, there is a break between the two most inboard slots and the outboard slots along the leading edge of approximately 75 mm because of structural constraints. The break is located where the outer-wing panel spar is connected to the inboard portion of the model.

Each disk is tuned to operate at a nominal 28-m/s peak velocity with a carrier frequency of 305 Hz. This carrier frequency was

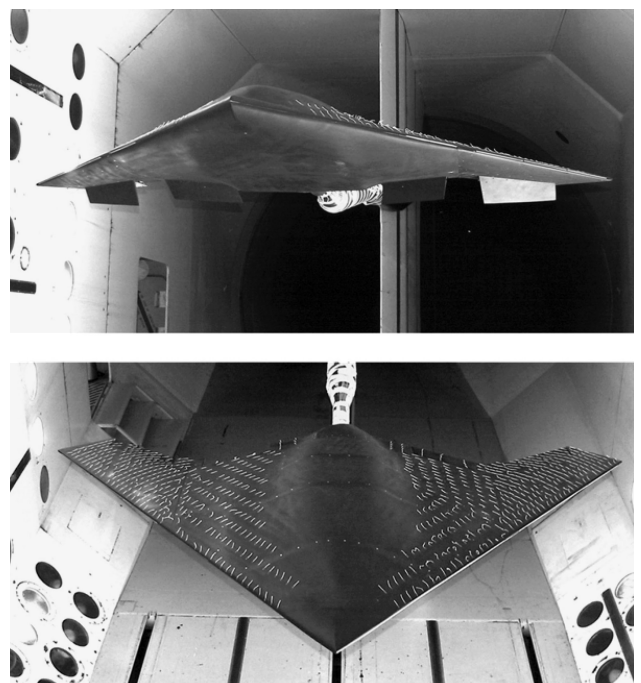


Fig. 1 Full-scale Stingray wind-tunnel model installed in NASA Transonic Dynamics Tunnel.

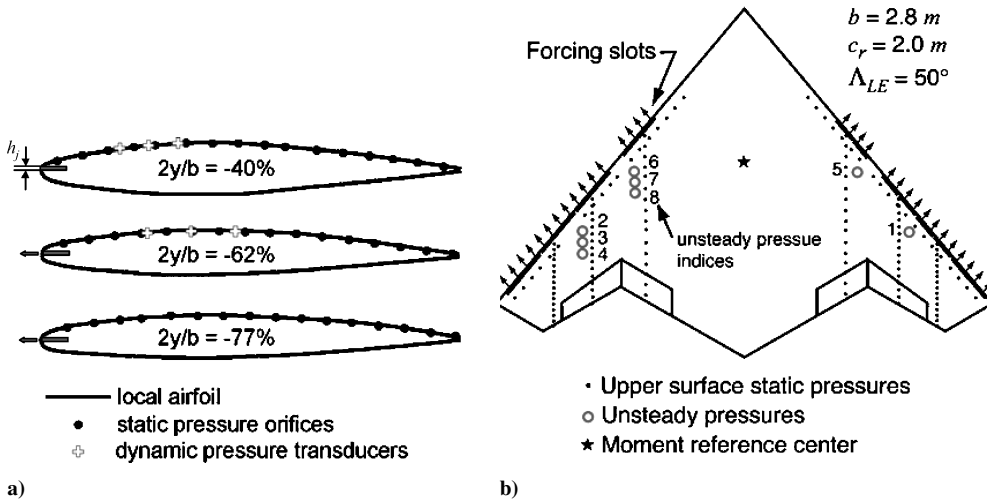


Fig. 2 Actuation and instrumentation locations on Stingray model.

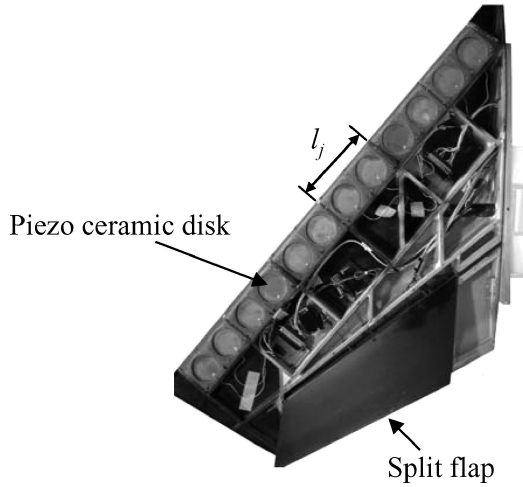


Fig. 3 Photo of the wing tip instrumented with array of synthetic jet actuators.

chosen such that it is an order of magnitude higher than the characteristic frequency of the flow (i.e., the time of flight based on the freestream velocity and the mean chord). This setting is considered the 100% power setting for the jets. The 305-Hz frequency is near the resonant peak of the piezoceramic disks, where all of the disks oscillate in phase. The actuator performance is measured using the momentum coefficient  $C_\mu$ :

$$C_\mu = \bar{I}_j / \frac{1}{2} \rho U_\infty^2 c_r \quad (1)$$

where  $\bar{I}_j$  is the time-averaged jet momentum per unit length during the outstroke and  $\rho$  is the freestream fluid density. The averaged momentum during the blowing cycle of the jet is

$$\bar{I}_j = \frac{1}{\tau} \rho_j h_j \int_0^\tau u_j^2(t) dt \quad (2)$$

where  $\tau = T/2$ ,  $T$  is the period of the diaphragm motion,<sup>12</sup>  $h_j$  is the jet orifice width, and  $u_j(t)$  is the phase-averaged velocity at the jet exit plane measured with a single hot-wire anemometry. During the course of the investigation, the jets were also operated with both amplitude modulation and pulse modulation at different modulation frequencies to change the character of the active flow control.

Figure 2 also illustrates the location of static-pressure ports on the model, the moment center location, and the location of eight dynamic-pressure transducers. The moment center corresponds to

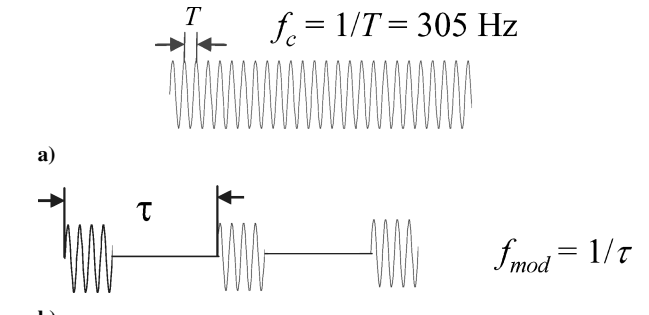


Fig. 4 Actuation waveforms: a) sinusoidal and b) pulse modulation.

44% of the root chord. Forces and moments were acquired via an internal six-component balance.

### III. Results

#### A. Vehicle Control at High Angles of Attack

At conditions where the flow is normally separated from the leading edge of the Stingray vehicle, the zero-mass jets are able to affect significant control forces on the vehicle when compared to the flaps. They also tend to improve the flap efficiency (i.e., higher pitch, roll, and yaw moments for a given flap deflection; see Ref. 24). Effective control through the use of active flow control was observed through the angle-of-attack range from 14 to 24 deg.

Previous work by Amitay and Glezer<sup>10</sup> on a two-dimensional airfoil showed that in order to achieve an improvement in the efficiency of resonant jet actuators a pulsed modulated excitation input should be used instead of a continuous sinusoidal waveform (Fig. 4). Because the actuators' carrier timescale is much shorter than the characteristic time of the flow, this has the effect of introducing an impulse to the flow with each cycle. The pulsed modulation frequency of successive bursts of the driving signal helps to "capture" the vorticity produced during the initial stages of the separation process on the suction side of the airfoil and thus delay separation and increase the time-averaged lift force. This technique is implemented in the present paper to improve the efficiency of the control over the three-dimensional wing. All of the modulated results presented herein are for single-cycle pulses at the carrier frequency.

Figures 5a–5i present the effect of different pulse modulation frequencies on the time-averaged pressure distributions at  $\alpha = 14$ , 17, and 23 deg and at 40, 62, and 77% semispan on the port wing. Note that the carrier frequency for all of the modulation cases is 305 Hz, corresponding to a  $Sr_c = 10$  where the length scale used is  $\bar{c}$  for this  $\alpha$  and  $U_\infty$ . The high carrier frequency was chosen such that it is at least an order of magnitude higher than the characteristic

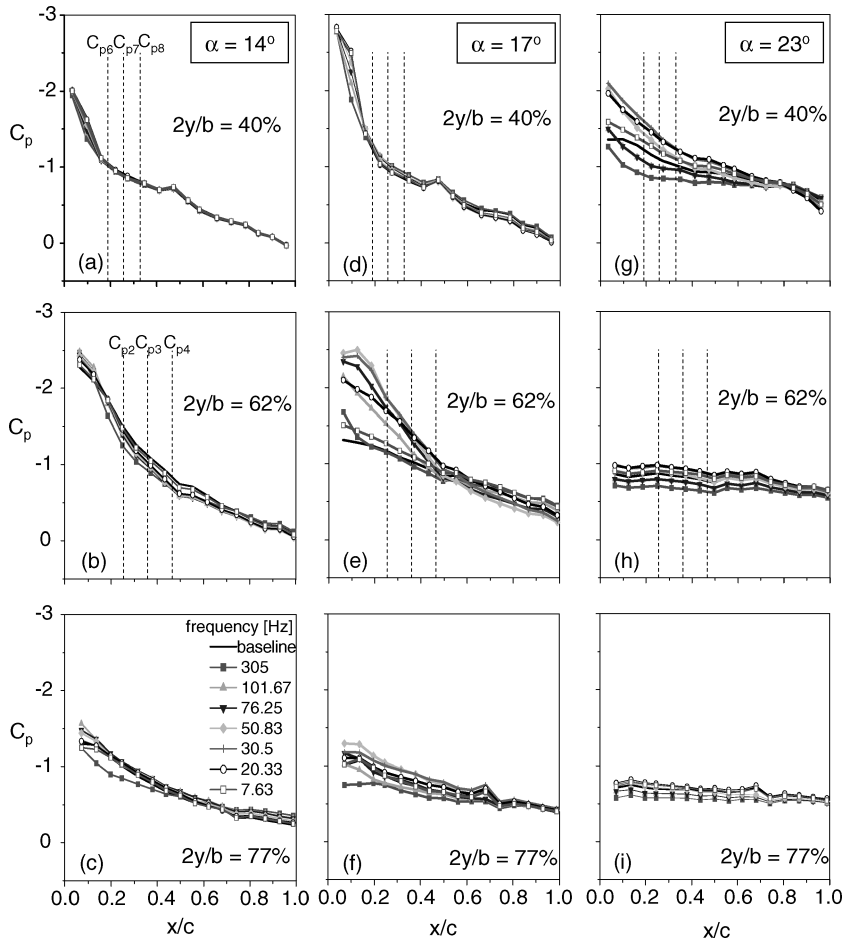


Fig. 5 Streamwise  $C_p$  distribution at a–c)  $\alpha = 14$  deg, d–f)  $\alpha = 17$  deg, and g–i)  $\alpha = 23$  deg; ----, locations of the dynamic pressure transducers.

frequency in the flow (following the work by Amitay and Glezer<sup>10</sup> on the effect of the actuation frequency on flow control effectiveness). The modulation frequencies were chosen such that it will be of the same order as the natural instability frequencies in the flow. The introduction of the modulation to the waveform has a profound effect on the pressure distribution on the upper side of the wing. However, at  $\alpha = 14$  deg and  $2y/b = 40\%$  the effect of the modulation is very small. At  $2y/b = 62$  and  $77\%$  (Figs. 5b and 5c) actuation results in an increase in the pressure along the chord, although there is a small increase in suction observed near the leading edge. The effect of the modulation is mostly noticeable at  $\alpha = 17$  deg and  $2y/b = 62\%$  (Fig. 5e), where the baseline flow is partially separated. When the synthetic jets are activated with a modulation frequency of 7.63 Hz the pressure is decreased (with respect to the baseline) from the leading edge to  $x/c \approx 0.5$ . As the modulation frequency is increased, the suction peak near the leading edge increases, where the largest effect is obtained at  $f_{\text{mod}} = 30.5$  and 50.83 Hz, which are of the same order of the frequency associated with the time of flight at this spanwise location,  $f_{\text{tof}} \approx 35$  Hz. Further increase of the modulation frequency results in a smaller suction peak, where the smallest effect is obtained for the no-modulation actuation (i.e., sine waveform). Furthermore, the downstream extent of the suction peak is also dependent on the modulation frequency; as the modulation frequency increases, the width of the suction peak decreases. This behavior is associated with the size of the interaction domain of the synthetic jet with the crossflow (see details in Ref. 10). The effect of the modulation is also noticeable at  $2y/b = 77\%$  (Fig. 5f), where the actuation yields a decrease and increase of the overall suction for high and low modulation frequencies, respectively. This behavior suggests that by simply changing the modulation frequency the lift force, as well as the pitching and rolling moments, can be increased or decreased with respect to the baseline values (for more details see

Fig. 6). Note that at this spanwise location, where the time of flight is shorter because of the smaller local chord, the best frequency shown for increase in suction is clearly the 50.83-Hz case.

At  $\alpha = 23$  deg (Figs. 5g–5i), where the baseline flow is almost completely separated at  $2y/b = 62$  and  $77\%$  and partially separated at  $40\%$ , the effect of the modulation is more pronounced further inboard (i.e., near the spanwise location of the separation,  $2y/b = 40\%$ ). Actuation with  $f_{\text{mod}}$  of 101.67 and 76.25 Hz results in a similar behavior as the sine wave actuation; except that the reduction in the suction peak is smaller. (There is a slight increase in pressure near the leading edge.) Lower modulation frequencies tend to increase the suction peak (as for  $\alpha = 17$  deg). However, the range of the most effective modulation frequency is slightly shifted toward smaller frequencies, corresponding to the larger local chord at  $2y/b = 40\%$ . Furthermore, at  $f_{\text{mod}} < 76.25$  Hz the flow seems to be completely attached to the upper surface of the wing in the time-averaged sense. At  $2y/b = 62$  and  $77\%$  (Figs. 5h and 5i) the modulation does not result in flow reattachment; however, the suction on the upper side is increased suggesting the severity of the separation is smaller.

As discussed in the preceding paragraph, pulse modulation actuation results in redistribution of the pressure on the wing suggesting that the moments and forces are altered. The lift, drag, the change in the rolling moment, and the pitching-moment coefficients were measured using a six-component balance and are presented in Figs. 6a–6d, respectively, as a function of the modulation frequency. In these cases, the leading-edge separation control is applied on all of the jets on the port wing only. The outboard starboard flap is deflected 10 deg, resulting in a negative rolling moment in the absence of leading-edge actuation. Each plot includes four angles of attack ( $\alpha = 14, 17, 20$ , and  $23$  deg), where the dashed lines represent the values of the corresponding baseline cases. For all cases the changes

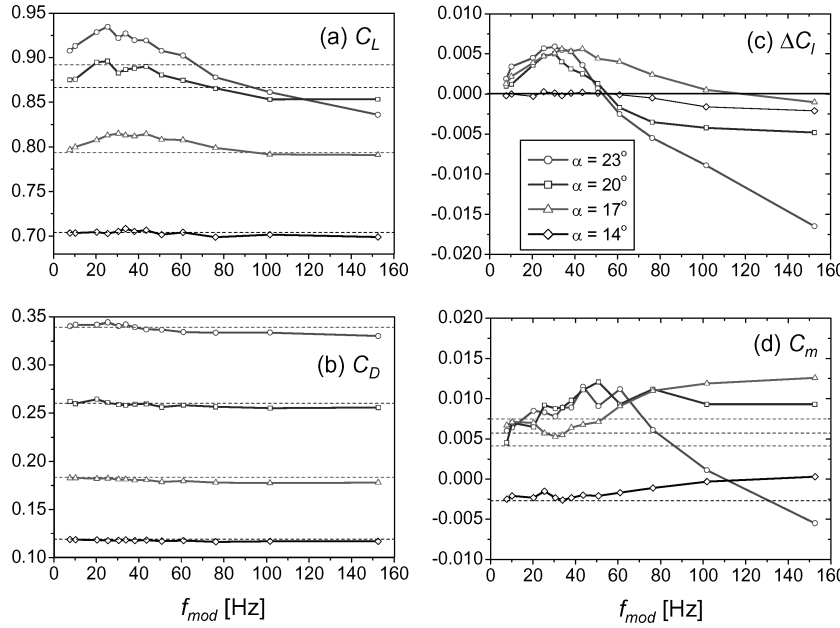


Fig. 6 Change of a) lift coefficient, b) drag coefficient, c) roll moment, and d) pitch-moment control with modulation frequency.

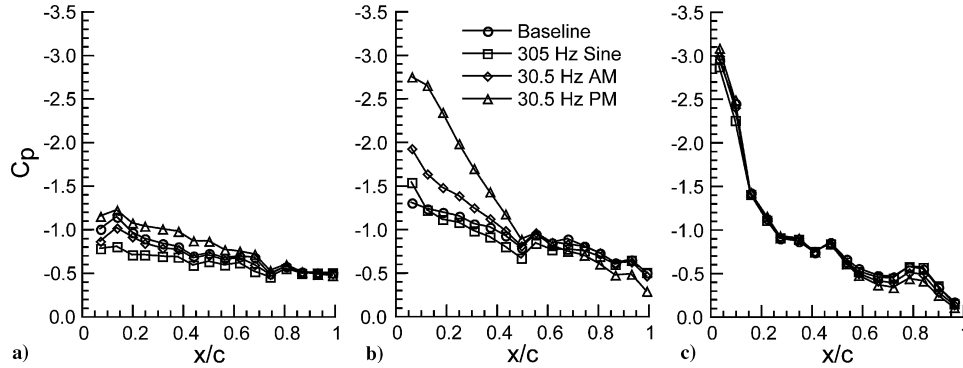


Fig. 7 Streamwise  $C_p$  distribution at  $2y/b$  = a) 77%, b) 62%, and c) 40%.

in the lift and drag coefficient are very small: an increase of the lift coefficient by up to 4% and a decrease of  $\sim 7\%$  at high  $\alpha$ . Along with the lift increment can be a drag coefficient change of  $\sim 1\%$  with respect to the baseline. However, these small lift and drag increments result in large pitch and roll moments as shown in Figs. 6c and 6d.

Figure 6c presents the effects of the actuation on the change in the rolling moment  $\Delta C_l$ . At  $\alpha = 14$  deg, the change in  $C_l$  is hardly noticeable. At higher angles of attack, as the  $f_{\text{mod}}$  is increased from low frequencies to high frequencies,  $\Delta C_l$  initially increases corresponding to increased suction on the port wing and opposite to the starboard flap effect. At each angle there is a  $f_{\text{mod}}$  where the trend reverses, and as  $f_{\text{mod}}$  is further increased the suction on the port wing actually decreases. (At  $\alpha = 20$  and 23 deg,  $\Delta C_l$  becomes negative, i.e., below its baseline value without control.) Therefore, the sign of the increment in  $\Delta C_l$  can be reversed merely by changing  $f_{\text{mod}}$ . Note that the increments on  $C_l$  as a result of active separation control are larger than the increment caused by the (10-deg) deflected flap for  $\alpha > 14$  deg. The Stingray stalls from the wing tips as  $\alpha$  increases; thus, separation control is more effective on the outboard wing at this angle. However, there is also less planform area contributing to the loads on the outboard wing (see Fig. 2).

The effect of the modulation frequency on the pitching moment  $C_m$  is shown in Fig. 6d. At  $\alpha = 14$  deg, the pitching moment linearly increases (less stable) as  $f_{\text{mod}}$  increases. At  $\alpha = 17$  deg, where leading-edge separation is more predominant in the baseline flow, the pitching moment is smaller than the baseline case for  $f_{\text{mod}} < \sim 45$  Hz and larger for higher  $f_{\text{mod}}$ . At higher angles of attack, as  $f_{\text{mod}}$  increases  $C_m$  is initially increased and it decreases for higher

$f_{\text{mod}}$  (for  $f_{\text{mod}} > 43$  and 50 Hz at  $\alpha = 20$  and 23 deg, respectively). Note that the initial slope of  $C_m$  with increasing  $f_{\text{mod}}$  is indicative of the location along the leading edge of the most effective separation control with respect to the moment center shown in Fig. 2. Note that active flow control on only one wing is used in these data. Clearly, more vehicle control authority could be obtained by using active flow control on both wings.

The effect of the input waveform was also investigated for three different actuation waveforms. Time-averaged pressure distributions measured using static-pressure ports at 77, 62, and 40% semispan on the port wing are shown in Figs. 7a–7c, respectively. The first is a sinusoidal waveform at the carrier frequency  $f_c$  of 305 Hz. The second waveform is an amplitude-modulation (AM) signal with  $f_{\text{mod}}$  exactly one order of magnitude less than  $f_c$ . The third waveform is a 25% duty-cycle pulse-modulation (PM) signal at the same  $f_{\text{mod}}$  as the AM signal. In these cases the model is at  $\alpha = 17$  deg with all of the flaps deflected symmetrically at  $\delta_f = 10$  deg. At this condition, the surface-pressure data indicate that the flow is attached at the 40% semispan row of pressure ports but separated at both 62 and 77% semispan (Figs. 5d–5f).

At 77% semispan (Fig. 7a) the baseline flow is clearly separated for  $x/c > 0.4$ . When a sine wave excitation is applied, the suction pressure is reduced, and hence the sectional lift is reduced (compared to the baseline flow). The AM waveform also results in less suction pressure than the baseline flow, however, the change is very small. However, the PM waveform yields an increase in upper surface suction and therefore an increase in sectional lift. Note that the trailing-edge pressures are equivalent in each case and that the

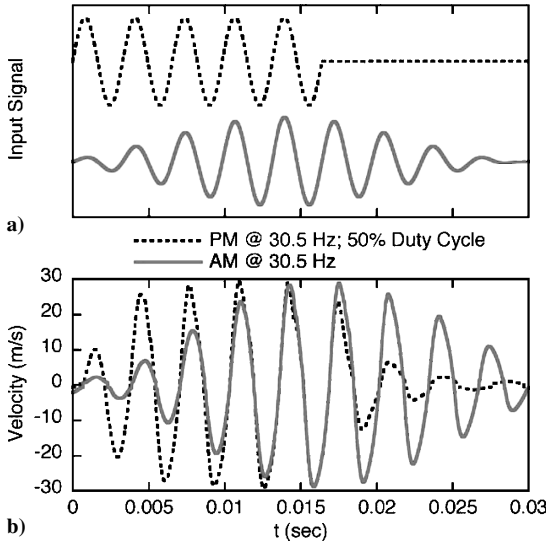


Fig. 8 Effect of waveform: a) input waveforms and b) velocity at the jet exit plane vs time.

general shape of the curves near the leading edge is similar for the baseline and modulated waveforms.

The effect of leading-edge separation control is more pronounced at the 62% semispan location as shown in Fig. 7b. Again, the sine wave excitation at  $Sr_c = 10$  resulted in a slight decrease in suction pressure along the chord. However, the most forward pressure port indicated an increase in suction near the leading edge. The PM waveform is more effective in increasing sectional lift than the AM waveform at the same  $f_{\text{mod}}$  corresponding to  $Sr_c = 1$ . In the case of the PM waveform, the trailing-edge condition has also changed, indicating a more global effect.

At the 40% semispan location (Fig. 7c), the flow is attached at this  $\alpha$  and  $U_\infty$ . There is little effect of the leading-edge actuation on the time-averaged surface pressures, although the slight differences seen on the leading two pressure ports follow the trends observed at the outboard pressure port rows.

The reason why the AM actuation is less effective (in terms of large increases in suction pressure) than PM actuation can be deduced from the wind-off calibration of the exit velocities as measured by a hot-wire probe. The velocities were measured at the jet's exit plane and were derectified to account for the reverse flow (during the suction portion of the cycle) at the orifice. The differences in actuator output based on input function are shown in Figs. 8a and 8b. The input signal is shown in Fig. 8a, with the resulting derectified velocities shown in Fig. 8b. The two waveforms are equivalent in terms of input energy. Two characteristics are evident in the velocity traces. First, the PM actuation results in a more rapid impulse to the flow. Second, in the case of the PM actuation  $f_c$  is present only during the pulse duration. In AM actuation the  $f_c$  frequency is present throughout the duration of the waveform.

## B. Flow Response to Actuation

The main goal of this paper is to understand the dynamic processes of the controlled flow that are affected using synthetic jet actuators and what the key processes are. First, the dynamic response of the system following a step function amplitude modulation of the actuator (control) input is considered. As before, the carrier frequency is 305 Hz and is kept constant during the experiments. Throughout the remainder of the discussion, the actuation signal is either a sine wave at the actuator carrier frequency of 305 Hz or pulse modulated with the modulation frequency ranging from 7.63 to 101.67 Hz.

Initially, the importance of the duty cycle (or energy input) is investigated for a modulation frequency of 30.5 Hz and duty cycles of 25% (dashed line) and 10% (solid line) and is shown in Figs. 9a and 9b. (The sinusoidal waveform is shown for reference using dashed-dot line.) Note that at this combination of modulation and carrier frequencies 10% duty cycle corresponds to a single pe-

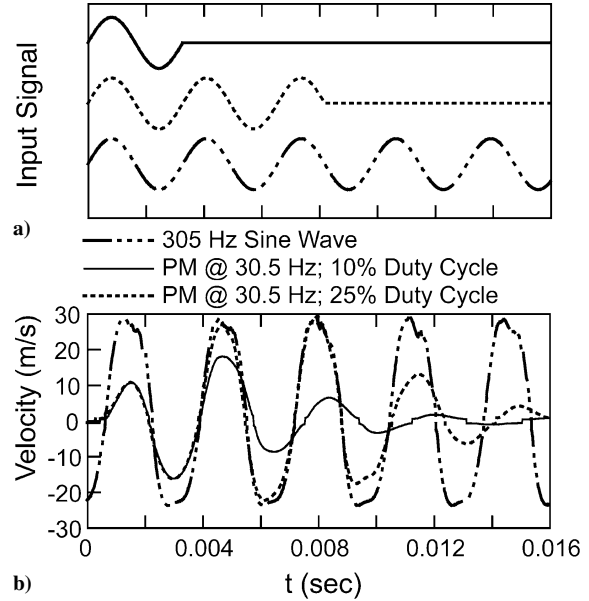


Fig. 9 Effect of duty cycle: a) input waveforms and b) velocity at the jet exit plane vs time.

riod of the carrier frequency per pulse. Figure 9a shows the various input waveforms, while Figure 9b presents the velocity time traces of the synthetic jet measured at the jet exit plane. These velocity traces were acquired with a hot-wire anemometer and were derectified to indicate the reverse velocity during the suction portion of the cycle. Note that there is a phase lag in the response of the actuators to the input signal, which might be caused by the capacitance of the disks and the associated electronic hardware. The sinusoidal waveform results in a periodic velocity variation with a peak of about 28 m/s. However, the actuator response to the pulse modulation signals can be described as a decaying wave packet having a characteristic frequency that is approximately equal to the carrier frequency. For the 25% duty-cycle pulse modulation waveform the velocity reaches the same peak velocity as for the continuous sine waveform by the blowing portion of the second cycle. In the case of the single cycle waveform, the first cycle velocity trace is identical to the first cycle of the 25% duty cycle; however, the peak velocity is reduced to approximately 18 m/s after the input signal is terminated. The peak is on the second cycle of the disk actuator motion because of the resonance of the system at the carrier frequency.

Given the information presented in Fig. 9b from the wind-off calibration of the leading-edge control jets, the effect of varying the duty cycle between 10 and 25% at  $f_{\text{mod}}$  of 30.5 Hz is considered. The transient response of the flow over the wing to the leading-edge actuation was acquired using phase-locked measurement of the transitory pressure coefficient via dynamic surface-pressure transducers. The phase-averaged response of the surface pressure at eight locations was computed from ensembles each comprised of 50 realizations that were measured phase locked to the modulating waveform through a 2-s period. Data were obtained for 0.5 s, before the control was initiated, during 1 s of actuation, and for 0.5 s after actuation was terminated.

Figure 10 presents a comparison of the normalized surface pressure between the two actuation cases (10 and 25% duty cycle) at an angle of attack of 16 deg. Here, the change in the unsteady surface pressure (with respect to the uncontrolled baseline condition) at location 2 is presented; however, similar results were obtained for all other pressure locations. Clearly, the transients associated with the activation and termination of the control as well as the quasi-steady behavior during control input are almost identical for both actuation waveforms. However, the 10% duty cycle requires only 40% of the energy input into the system for the same level of control. Furthermore, based on the wind-off jet calibrations presented in Fig. 9b, it is concluded that it is the impulse to the system that

is most important for a given level of control, and any additional energy input in succeeding cycles is a waste.

Because of the effectiveness of the single-cycle pulse modulated input, only the results where the actuation waveform corresponds to single-cycle pulse modulation are presented in the following discussions, where the duty cycle varies based on the ratio of  $f_{\text{mod}}/f_c$ .

### 1. Sine Wave Actuation

First, we investigated the dynamic response of the system following a step function of the actuator (control) input, where the input

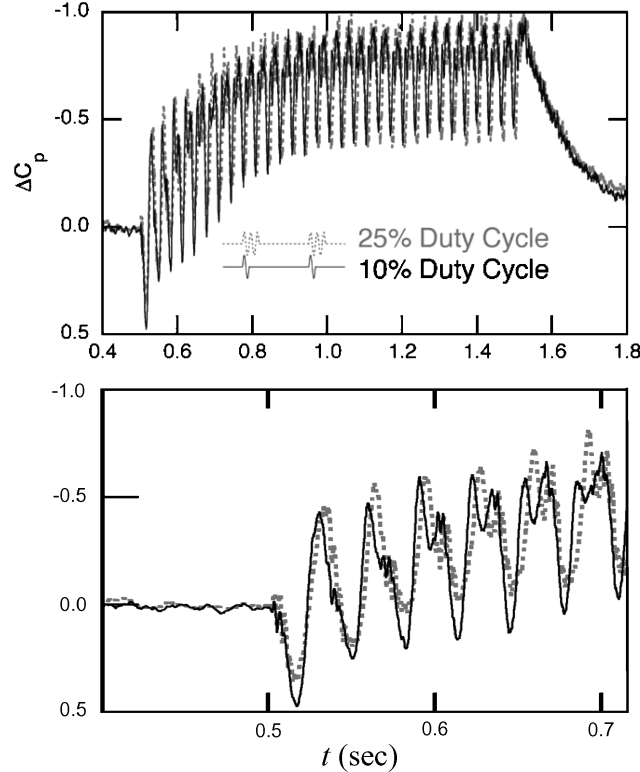


Fig. 10 Time variation of the normalized surface pressure for two actuation duty cycles of 10 and 25% at an angle of attack of 16 deg.

waveform is sinusoidal with a driving frequency of 305 Hz. The phase-averaged response of the surface pressure at the eight locations was computed from ensembles each composed of 50 realizations that were measured phase locked to the modulating waveform through a 2-s period. Data were obtained for 0.5 s before the control was initiated, during 1 s of actuation and for 0.5 s after actuation was terminated.

Figures 11a–11e present the time dependence of the change of the normalized phase-averaged surface pressure (with respect to the uncontrolled baseline values) at  $\alpha = 14, 18. Each plot includes data for three transducers based on the span location. Note that the data were shifted vertically for better viewing, and the up and down arrows represent the times when the control was turned on and off, respectively.$

At the outboard locations (locations 2, 3, and 4 and a, c, and e), which are closer to the separation location, activation and termination of the control result in large oscillations in the surface pressure. However, the intensity and duration of the oscillations are different at the various angles of attack. At  $\alpha = 14\text{ deg}$  (Fig. 11a), where the baseline flow appears to be attached upstream of  $x/c = 0.85$  (Fig. 5), pressure exhibits a large overshoot before reaching to the quasi-steady controlled value following the transients. When control is terminated, the pressure oscillates (there is a small overshoot followed by a larger increase in pressure) before it approaches its uncontrolled value. During actuation, the mean of the quasi-steady pressure is slightly increased, which corresponds to the data shown in Fig. 4b.

At higher angles of attack ( $\alpha = 18$  and  $24\text{ deg}$ ; Figs. 11c and 11e), where the extent of the separation region is larger, the transients associated with the activation and deactivation of the control are longer and include several periods before reaching their quasi-steady values. This transient response behavior is likely caused by baseline flow being separated at these locations and angles of attack (Fig. 5). The frequency of this transient oscillation appears to be near the frequency associated with the characteristic time of the flow  $f_{\text{tot}}$ . As the actuation continues, the forcing overpowers the natural tendencies of the dynamic flow processes.

At locations 6, 7, and 8 (farther inboard) the control has an effect on the pressure at higher angles of attack, where the separation moves inboard. The transients associated with the activation of the control are similar to those at the outboard locations, except that they occur at higher angles of attack. For example, the transients for  $\alpha = 24\text{ deg}$  at location 8 are very similar to the transient for  $\alpha = 18\text{ deg}$  at location 6. However, at the inboard locations,

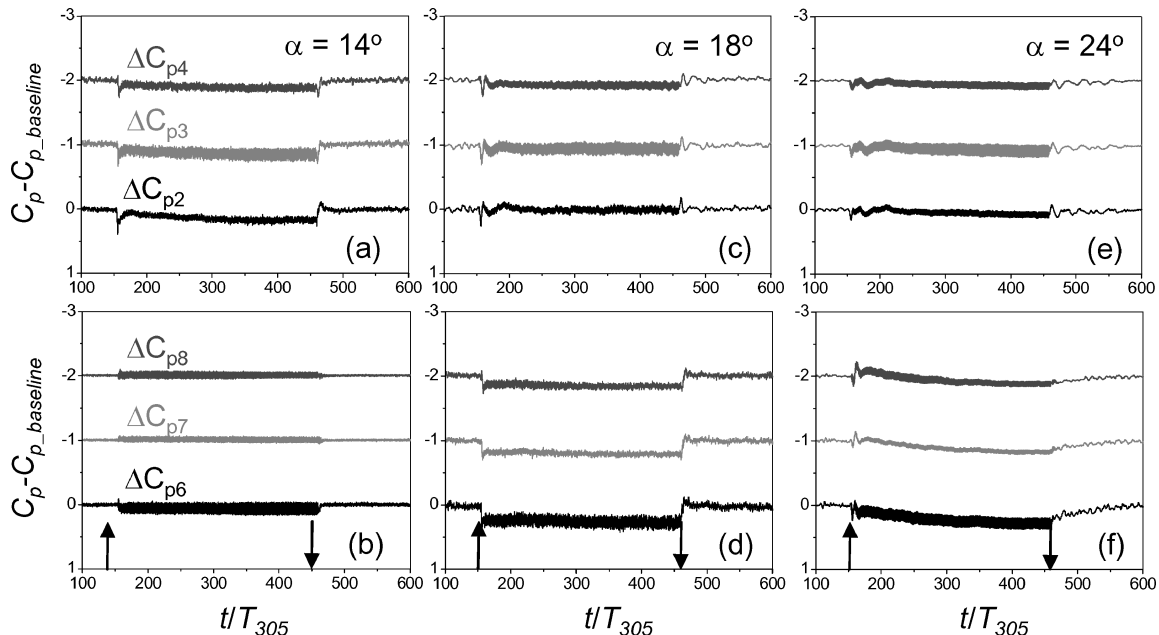


Fig. 11 Variation of the phase-averaged change of the pressure (with respect to the baseline value) with normalized time. Sinusoidal actuation: a, b)  $\alpha = 14\text{ deg}$ , c, d)  $\alpha = 18\text{ deg}$ , and e, f)  $\alpha = 24\text{ deg}$ .

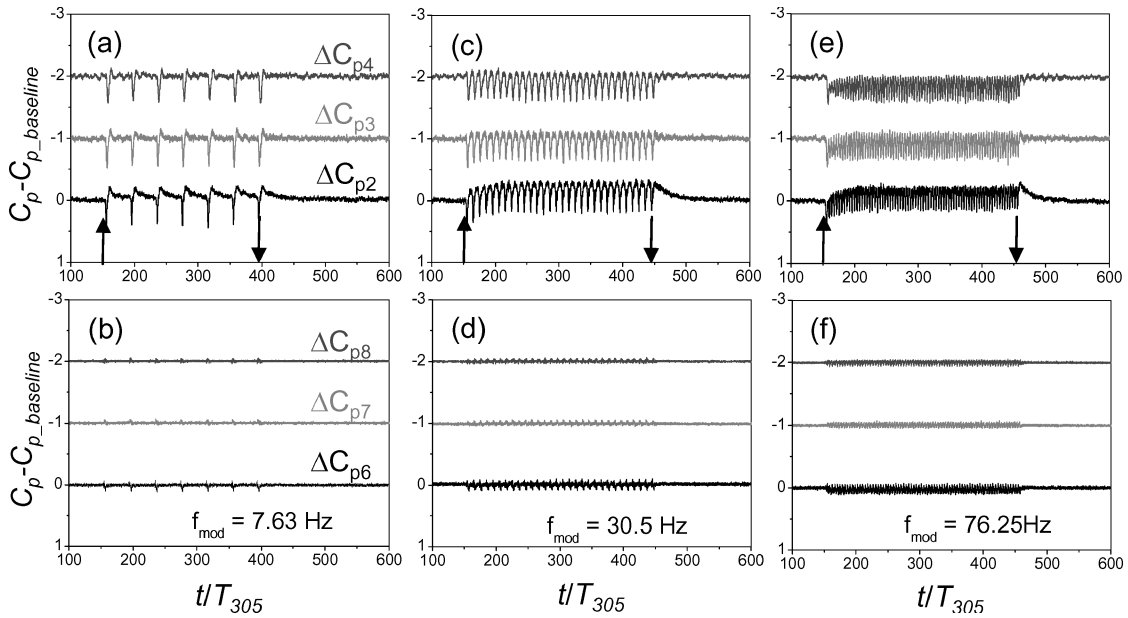


Fig. 12 Change of the phase-averaged pressure with normalized time at  $\alpha = 14$  deg. Pulsed-modulation actuation: a, b)  $f_{\text{mod}} = 7.63$  Hz, c, d)  $f_{\text{mod}} = 30.5$  Hz, and e, f)  $f_{\text{mod}} = 76.25$  Hz.

following the oscillations, it takes more time for the pressure to reach its quasi-steady attached value compared to the outboard pressure. This might be because of the larger separation length associated with the inboard pressure locations. For the same reasons, it takes the pressure field in the inboard locations more time to return to its uncontrolled value, when the control is terminated. Moreover, at all measurement locations, following the transients associated with the activation of the control, the pressure oscillates at the actuation frequency of 305 Hz. However, the magnitude of the periodic oscillations is relatively small (especially when compared to the oscillations associated with the pulse modulation actuation that is discussed in the next section).

## 2. Pulse Modulation Actuation

The time dependence of the change of the normalized phase-averaged surface pressure (with respect to the baseline value) as a result of pulse modulation actuation, measured at  $\alpha = 14$  deg, is shown in Figs. 12a–12f. Figures 12a, 12c, and 12e present the data for single-cycle pulse-modulated frequencies of 7.63, 30.5, and 76.25 Hz, respectively, for locations 2, 3, and 4 and Figs. 12a, 12d, and 12f the corresponding data for locations 6, 7, and 8, respectively. The flow is unforced before and after the pulse-modulated excitation is turned on and off (marked with up and down arrows on the timescale). At this angle of attack, the flow is attached to most of the upper surface of the wing (see Fig. 5), and actuation has only a small effect on the pressure distribution.

At  $f_{\text{mod}} = 7.63$  Hz (Figs. 12a and 12b) the effect of actuation is very small on the time-averaged pressures. It is apparent that at locations 2, 3, and 4 the surface pressure oscillates at the modulation frequency during the entire time that the control signal is applied. Notice that the magnitude of the oscillation decreases in the downstream direction (i.e., from location 2 to 3 to 4). The phase of each pulse of the modulating wave train is timed so that it retriggers separation just before the flow reaches steady state again following the reattachment process. This results in a small quasi-steady suction increment. The quasi-steady behavior of the pressure coefficient at locations 6, 7, and 8 is hardly affected by the actuation; there are small-amplitude oscillations, where the forced values are the same as the corresponding uncontrolled values. These results are not surprising because at this angle of attack the flow in the vicinity of locations 6, 7, and 8 is attached, whereas it is on the verge of separation near locations 2, 3, and 4.

When the modulation frequency is increased to 30.5 Hz (Figs. 12c and 12d), the elapsed time between pulses within the modulating

wave train is decreased, and the large oscillations in the circulation are somewhat attenuated. This suggests that the modulating pulses are better timed to prevent continuous shedding of large vortical structures and the corresponding variations in pressure. The recovery of an asymptotic change of pressure suggests that the actuation results in a larger increase in lift force with a larger accumulation and maintenance of (clockwise) vorticity on the suction side of the wing even though the reattachment is unsteady and the pressure oscillates with peak-to-peak variations of  $\sim 0.3$ . Further increase in the modulation frequency to 76.25 Hz (Figs. 12e and 12f) results in a smaller change in the piecewise-averaged pressure, with somewhat smaller oscillations. At this angle of attack, the most effective modulation frequency is 30.5 Hz, which corresponds to the natural frequency associated with the time of flight  $f_{\text{tot}}$ . The transients following the activation of the control (at location 2) are associated with a sharp and rapid increase in the pressure, whereas the termination of the control is associated with a much slower transient before it reaches to its uncontrolled value. However, at the other locations the transients associated with the termination of the control are very short because of the small effect of the actuation on the pressure coefficient.

At a higher angle of 18 deg (Figs. 13a–13f), the extent of the separation region of the baseline flow over the wing is larger. Therefore, the effect of the pulse modulation actuation is more pronounced. The effect of the actuation is noticeable at all pressure locations presented. At low modulation frequency  $f_{\text{mod}} = 7.63$  Hz (Figs. 13a and 13b), actuation results in a decrease in the pressure, where the largest effect is at locations 2 and 6 (near the leading edge, see also Fig. 5 at  $\alpha = 17$  deg). Similar effects are obtained at  $f_{\text{mod}} = 30.5$  Hz (Figs. 13c and 13d); however, the effect of the control is larger (i.e., larger suction peak). Actuation with a modulation frequency of  $f_{\text{mod}} = 76.25$  Hz (Figs. 13e and 13f) results in an opposite effect (i.e., increase in the pressure) at most locations, except in location 2. Apparently, at this modulation frequency the forcing is too fast for the flow to respond like it does at 30.5 Hz. This behavior is similar to the effects of high modulation frequency on a two-dimensional airfoil observed by Amitay and Glezer.<sup>10</sup> Moreover, at locations 2, 3, and 4 the transients associated with the activation of the control results in a rapid increase in the pressure followed by a larger decrease in pressure (with a characteristic frequency of approximately 30 Hz) before converging to the quasi-steady controlled value. Similar to the transients that are associated with the arrival of the leading edge of the pulse at the measurement locations, the arrival of its trailing edge affects the pressure field. The

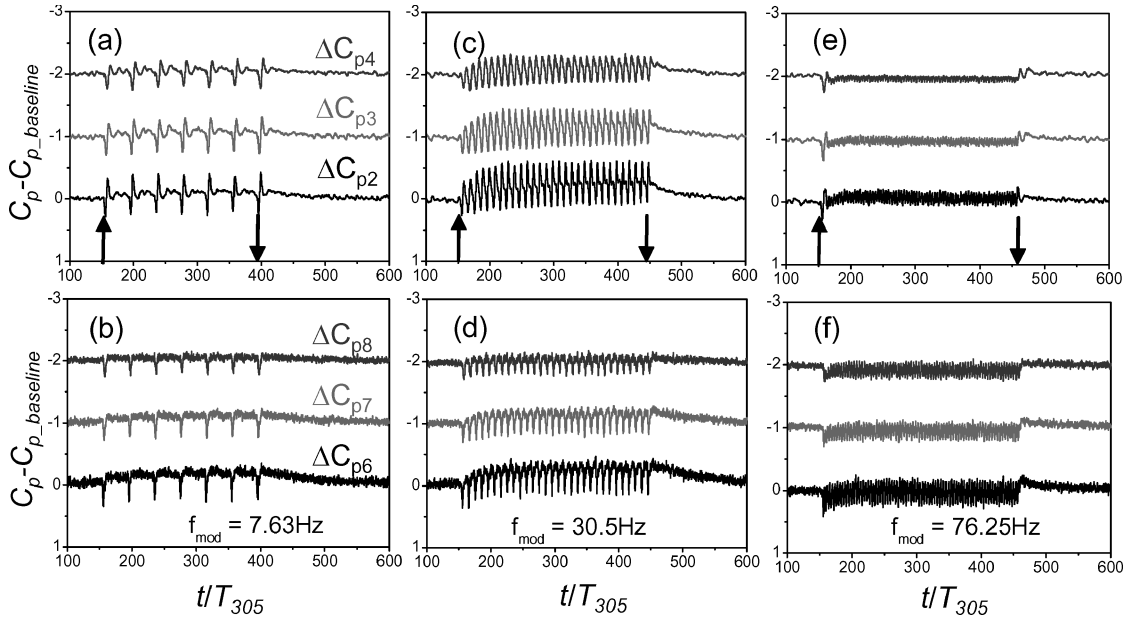


Fig. 13 Change of the phase-averaged pressure with normalized time at  $\alpha = 18$  deg. Pulsed-modulation actuation: a, b)  $f_{\text{mod}} = 7.63$  Hz, c, d)  $f_{\text{mod}} = 30.5$  Hz, and e, f)  $f_{\text{mod}} = 76.25$  Hz.

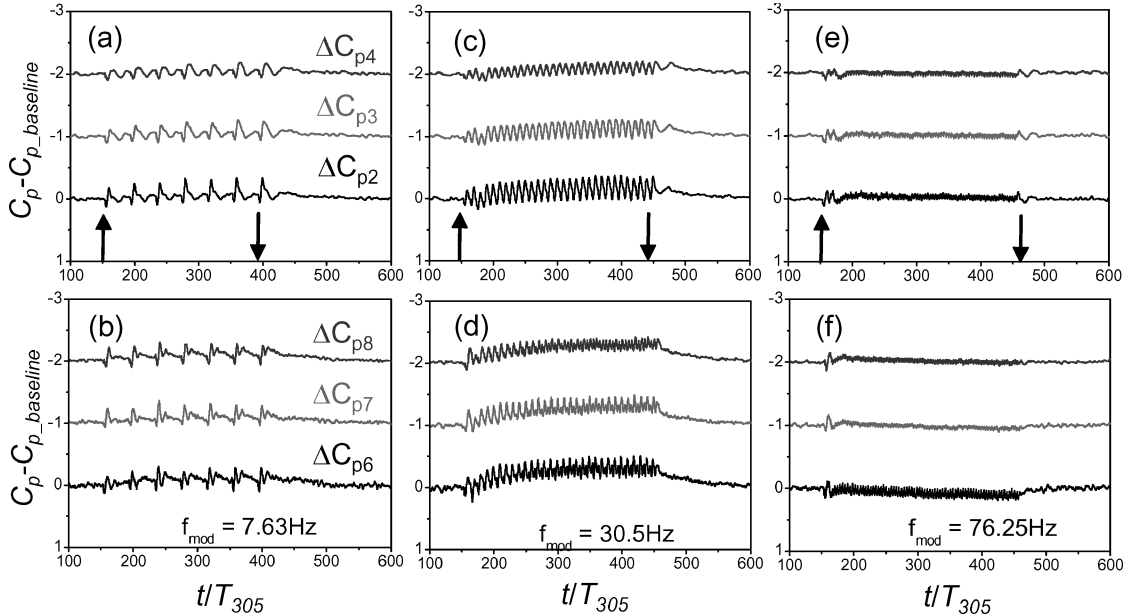


Fig. 14 Change of the phase-averaged pressure with normalized time at  $\alpha = 24$  deg. Pulsed-modulation actuation: a, b)  $f_{\text{mod}} = 7.63$  Hz, c, d)  $f_{\text{mod}} = 30.5$  Hz, and e, f)  $f_{\text{mod}} = 76.25$  Hz.

termination of the control is also associated with oscillations; however, these transients are slightly slower having a characteristic frequency of approximately 20 Hz. At locations 6, 7, and 8, which are farther from the separation location, the transients when the control is turned on or off are more rapid and do not exhibit any noticeable oscillations.

The time dependence of the change in the normalized surface pressure at a higher angle of 24 deg is presented in Fig. 14 for modulation frequencies of 7.63, 30.5, and 76.25 Hz. Applying the control with a modulation frequency of 7.63 Hz (Figs. 14a and 14b) results in a decrease in the pressure on the upper side of the wing at all measurement locations. However, the effect is larger farther inboard (i.e., at locations 6, 7, and 8). Note the appearance of higher harmonics in the pressure distributions, which might be attributed to nonlinear mechanism of the vortical structures.

Similar to the lower angle-of-attack case (Figs. 13a–13f), when the modulation frequency is 30.5 Hz (Figs. 14c and 14d) the resulting quasi-steady pressure at locations 2, 3, and 4 exhibits oscillatory behavior. However, the oscillations seem to have more of a sinusoidal shape than at  $\alpha = 14$  and 18 deg. The pressure waveform suggests that the actuation wave train is not optimal, resulting in retriggering of reattachment before the flow separates again. Furthermore, the change in the pressure coefficient at this location is much smaller than at 18 deg, which can be attributed to the fact that at 24 deg the separation is more severe where the flow is separated farther inboard (i.e., farther upstream). Moreover, at locations 6, 7, and 8 where the actuation with 30.5-Hz frequency modulation at an angle of attack of 18 deg had a small effect on the pressure, at 24 deg the actuation results in a larger decrease in the pressure. Furthermore, the magnitude of the oscillations is smaller, and higher harmonics develop over

the course off the actuation cycle. This behavior suggests that this modulation frequency is more effective at locations 6, 7, and 8. At this high angle of attack, actuation with  $f_{\text{mod}} = 76.25$  Hz (Figs. 14e and 14f) results in a very small effect on the pressure field. However, the transients associated with the activation and termination of the control are very similar to the lower modulation frequency (Figs. 14c and 14d).

To verify that the unsteady wall-pressure data presented in Figs. 10–14 are actually caused by the flow and not structural vibration or sound field exerted by the synthetic jet actuators, the unsteady pressures were measured in the absence of freestream with the synthetic jets turned on. Figure 15 presents a comparison of the change in the dimensional pressure at location 2 with and without flow subjected to actuation with a modulation frequency of 30.5 Hz. The figure presents the input waveform (in arbitrary units) and the unsteady dimensional pressures (psi) with the flow off and with the flow on at  $\alpha = 14, 16, 18$ , and 24 deg. Clearly, the effect of the actua-

tion on the wind-off pressure transducers data is minimal compared to the magnitude of the oscillations when the flow is on. Thus, it is concluded that the periodic nature of the pressure is caused by the effect of actuation on the flow and is not a structural/sound effect. Note that the same behavior was observed for different modulation frequencies and for the other pressure transducers.

The change of the pressure coefficients at locations 2 and 6 (with respect to the baseline values) with the modulation frequency is presented in Figs. 16a and 16b, respectively, at different angles of attack. At location 2 (Fig. 16a) the maximum change in the pressure coefficient occurs at a modulation frequency of 30.5 Hz for the four angles of attack presented, where the change in  $\Delta C_p$  is smaller for lower and higher modulation frequencies. However, at location 6 the dependence of the surface pressure on the modulation frequency is quite different; at  $\alpha = 14$  and 16 deg increasing the modulation frequency increases the change in the surface pressure where the maximum change is obtained for the periodic actuation of 305 Hz (without modulation). This can be attributed to the fact that at this location the flow is attached and modulation frequency is not effective, whereas the high-frequency control results in a local modification of the flowfield (similar to the effects reported by Honohan et al.<sup>25</sup> on a circular cylinder). However, at higher angles of attack ( $\alpha = 18$  and 24 deg), where the flow at location 6 is separated, the dependence of the surface pressure with modulation frequency is similar to that of location 2 at lower angles of attack.

#### IV. Conclusions

An experimental investigation of the physical processes and interactions caused by leading-edge separation control on a 50-deg swept uninhabited air vehicle (UAV) have been presented. Flow control via arrays of synthetic jet actuators has been implemented where the control jets are mounted along the leading edges of the wing. The synthetic jet effectiveness on the global aerodynamic performance was investigated at angles of attack between 14 and 24 deg and for different actuation waveforms.

At conditions where the flow is normally separated from the leading edge of the Stingray vehicle, the zero-mass jets were able to create significant control forces and moments on the vehicle when compared to the flaps. Effective vehicle control using active flow control was observed through the entire range of angles of attack tested.

The main goal of the present work is understanding the dynamic processes of the controlled flow over the UAV that are affected using synthetic jet actuators and what the key processes are. To do so, the dynamic response of the system following a step function amplitude modulation of the actuator (control) input was considered. The carrier frequency was 305 Hz and was kept constant during the experiments, where the actuation signal was either a sine wave at the actuator carrier frequency of 305 Hz or pulse modulated with the modulation frequency ranging from 7.63 to 101.67 Hz.

The transient behavior is not the same for different angles of attack as well as at different downstream locations on the wing. At moderate angles of attacks, the transient pressure data on the outboards of the wing (where the flow is separated) are very similar to the transients associated with reattachment over a stalled two-dimensional airfoil. Following the transients, the surface pressure continues to oscillate at the modulation frequency during the entire time that the control signal is applied. However, the magnitude of the oscillation decreases as the modulation frequency increases.

The pressure transients in the inboard section are quite different; following the onset of the control, the pressure changes rapidly to its actuated value without the large oscillation. This can be attributed to the attached flow at the location of the measurement. The activation of the control results in a suction peak near the leading edge; however, while excitation with a sine waveform results in a sharp suction peak near the leading edge, pulse modulation yields a larger and wider suction peak. As the modulation frequency decreases, the size of the suction peak increases where the highest magnitude is achieved for  $f_{\text{mod}} = 43.6$  Hz, which corresponds to the natural frequency of the separated flow over the wing. Furthermore, in all of the pulse-modulation waveforms the trailing-edge condition has also changed, indicating a more global effect.

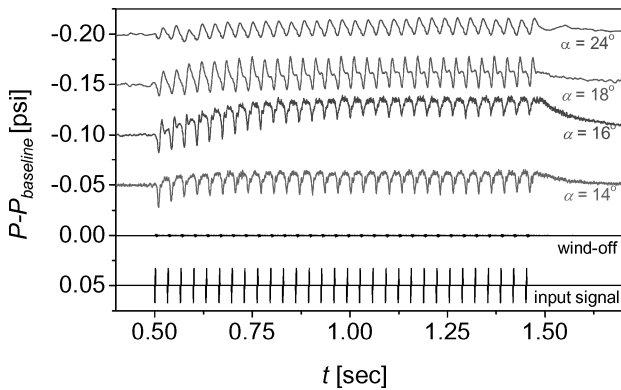


Fig. 15 Time variation of the transducer's pressure with and without flow. The input signal is shown on the bottom for reference.

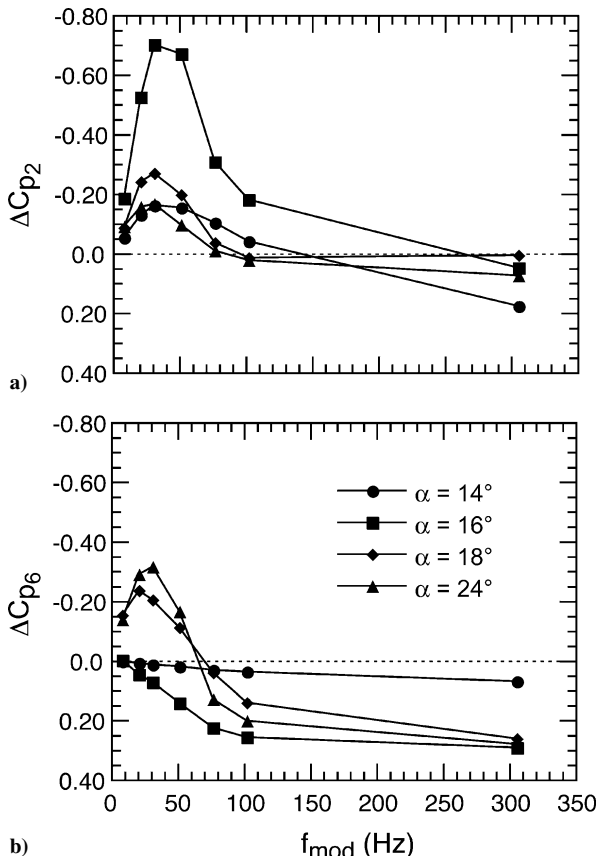


Fig. 16 Change in average  $C_p$  (with respect to the baseline values) at locations 2 and 6 as function of modulation frequency.

## Acknowledgments

This research was performed (in part) under Contract #NAS1-00087 as part of Morphing Project at NASA Langley Research Center. The authors greatly appreciate the contributions of Steve Williams, Warren Lee, and Shayne Kondor and the fruitful discussions with Ari Glezer.

## References

- <sup>1</sup>Ho, C.-M., and Huerre, P., "Perturbed Free Shear Layers," *Annual Review of Fluid Mechanics*, Vol. 16, 1984, pp. 365–424.
- <sup>2</sup>Oster, D., and Wygnanski, I. J., "The Forced Mixing Layer Between Parallel Streams," *Journal of Fluid Mechanics*, Vol. 123, 1982, pp. 91–130.
- <sup>3</sup>Roberts, F. A., "Effects of Periodic Disturbances on Structure of Mixing in Turbulent Shear Layers and Wakes," Ph.D. Dissertation, Div. of Engineering and Applied Science, California Inst. of Technology, Pasadena, CA, 1985.
- <sup>4</sup>Seifert, A., Darabi, A., and Wygnanski, I., "Delay of Airfoil Stall by Periodic Excitation," *Journal of Aircraft*, Vol. 33, No. 4, 1996, pp. 691–698.
- <sup>5</sup>Ahuja, K. H., and Burrin, R. H., "Control of Flow Separation by Sound," AIAA Paper 84-2298, Oct. 1984.
- <sup>6</sup>Neuberger, D., and Wygnanski, I., "The Use of a Vibrating Ribbon to Delay Separation on Two Dimensional Airfoils," *Proceedings of Air Force Academy Workshop in Unsteady Separated Flow*, edited by F. J. Seiler, Research Labs., Rept. TR-88-0004, U.S. Air Force Academy, Colorado Springs, CO, 1987.
- <sup>7</sup>Seifert, A., Bachar, T., Koss, D., Shepshelovich, M., and Wygnanski, I., "Oscillatory Blowing: A Tool to Delay Boundary-Layer Separation," *AIAA Journal*, Vol. 31, No. 11, 1993, pp. 2052–2060.
- <sup>8</sup>Wygnanski, I., "Some Observations Affecting the Control of Separation by Periodic Excitation," AIAA Paper 2000-2314, June 2000.
- <sup>9</sup>Amitay, M., Kibens, V., Parekh, D. E., and Glezer, A., "Flow Reattachment Dynamics over a Thick Airfoil Controlled by Synthetic Jet Actuators," AIAA Paper 99-1001, Jan. 1999.
- <sup>10</sup>Amitay, M., and Glezer, A., "Controlled Transients of Flow Reattachment over Stalled Airfoils," *International Journal of Heat Transfer and Fluid Flow*, Vol. 23, No. 5, 2002, pp. 690–699.
- <sup>11</sup>Amitay, M., Smith, D. R., Kibens, V., Parekh, D. E., and Glezer, A., "Modification of the Aerodynamics Characteristics of an Unconventional Airfoil Using Synthetic Jet Actuators," *AIAA Journal*, Vol. 39, No. 3, 2001, pp. 361–370.
- <sup>12</sup>Smith, B. L., and Glezer, A., "The Formation and Evolution of Synthetic Jets," *Physics of Fluids*, Vol. 10, No. 9, 1998, pp. 2281–2297.
- <sup>13</sup>Glezer, A., and Amitay, M., "Synthetic Jets," *Annual Review of Fluid Mechanics*, Vol. 34, 2002, pp. 503–529.
- <sup>14</sup>Cater, J. E., and Soria, J., "The Evolution of Round Zero-Net-Mass-Flux Jets," *Journal of Fluid Mechanics*, Vol. 472, 2002, pp. 167–200.
- <sup>15</sup>Smith, B. L., and Glezer, A., "Jet Vectoring Using Synthetic Jets," *Journal of Fluid Mechanics*, Vol. 458, 2002, pp. 1–34.
- <sup>16</sup>Kondor, S., Amitay, M., Parekh, D. E., Fung, P., and Glezer, A., "Active Flow Control Application on a Mini Ducted Fan UAV," AIAA Paper 2001-2440, 2001.
- <sup>17</sup>Fung, P., and Amitay, M., "Active Flow Control Application on a Mini Ducted Fan UAV," *Journal of Aircraft*, Vol. 39, No. 4, 2002, pp. 561–571.
- <sup>18</sup>Smith, D. R., Amitay, M., Kibens, V., Parekh, D. E., and Glezer, A., "Modification of Lifting Body Aerodynamics Using Synthetic Jet Actuators," AIAA Paper 98-0209, 1998.
- <sup>19</sup>Darabi, A., and Wygnanski, I., "Active Management of Naturally Separated Flow over a Solid Surface, Part I: Control of Reattachment," *Journal of Fluid Mechanics*, Vol. 510, 2004, pp. 105–129.
- <sup>20</sup>Darabi, A., and Wygnanski, I., "Active Management of Naturally Separated Flow over a Solid Surface, Part II: Control of Separation," *Journal of Fluid Mechanics*, Vol. 510, 2004, pp. 131–144.
- <sup>21</sup>Nain, A., Greenblatt, D., Seifert, A., and Wygnanski, I., "Active Control of Cylinder Flow with and Without a Splitter Plate Using Piezoelectric Actuators," AIAA Paper 2002-3070, 2002.
- <sup>22</sup>Pack, L., Yao, C. S., and Seifert, A., "Active Control of Separation from the Flap of a Supercritical Airfoil," AIAA Paper 2003-4005, 2003.
- <sup>23</sup>Margalit, S., Greenblatt, D., Seifert, A., and Wygnanski, I., "Active Flow Control of a Delta Wing at High Incidence Using Segmented Piezoelectric Actuators," *Journal of Aircraft* (to be published); also AIAA Paper 2002-3270, June 2002.
- <sup>24</sup>Parekh, D. E., Williams, S., Amitay, M., Glezer, A., Washburn, A. E., Gregory, I., and Scott, R. C., "Synthetic Jet Aerodynamic Control on a Full-Scale UAV," AIAA Paper 2003-4002, 2003.
- <sup>25</sup>Honohan, A., Amitay, M., and Glezer, A., "Aerodynamic Control Using Synthetic Jets," *AIAA Journal* (to be published); also AIAA Paper 2000-2401, 2000.

A. Karagozian  
Associate Editor